PHYSICAL REVIEW B **79**, 155441 (2009)

Critical and excess current through an open quantum dot: Temperature and magnetic-field dependence

H. I. Jørgensen,* K. Grove-Rasmussen,† K. Flensberg, and P. E. Lindelof
Nano-Science Center, Niels Bohr Institute, University of Copenhagen, Universitetsparken 5, DK-2100 Copenhagen Ø, Denmark
(Received 22 December 2008; revised manuscript received 27 March 2009; published 27 April 2009)

We present measurements of temperature and magnetic-field dependence of the critical current and excess current in a carbon nanotube Josephson quantum dot junction. The junction is fabricated in a controlled environment which allows for extraction of the full critical current. The measurements are performed in the open quantum dot regime and fitted to theory with good qualitative agreement. We also show how to extract level spacing, level broadening, and charging energy of an open quantum dot from a bias spectroscopy plot.

DOI: 10.1103/PhysRevB.79.155441 PACS number(s): 73.23.Ad, 74.45.+c, 73.63.Fg, 74.50.+r

I. INTRODUCTION

Nanoscale Josephson quantum dot junctions are intriguing devices showing several interesting physical phenomena. Supercurrent, Andreev reflections, quasiparticle transport, and excess current have all been studied in junctions where a nanotube,[1–9] nanowire,[10] or InAs island[11] constitute the quantum dot. Furthermore, the interplay between these Josephson-junction related phenomena and correlations as the Kondo effect[12–17] and the 0-π transition for more weakly coupled junctions has been explored.[3,18,19]

In this paper, we present experimental results in the strongly coupled regime for a Josephson quantum dot junction realized in a carbon nanotube. Inspired by Ref. 20, we utilize a designed external circuit in order to control the phase fluctuations which enables us to infer the true magnitude of the critical current, I_C, from the measurable critical current/switching current, I_m, by a fitting procedure.[18] I_m can significantly differ from I_C as demonstrated previously for nanotube-based Josephson junctions.[5,6,18] Here we analyze the magnetic-field dependence and temperature dependence of both the critical current and excess current.

II. DEVICE DESIGN

The devices are fabricated on a degenerately doped silicon wafer with a 0.5 μm layer of SiO_2. Carbon nanotubes are grown from islands of catalyst material and contacted by small electrodes of superconducting trilayers of 5 nm Ti, 60 nm Al, and 5 nm Ti. The superconducting electrodes are kept small to reduce junction capacitance. Each superconducting electrode is contacted by two normal-metal leads to bonding pads which enables four-probe measurements. The measurements are performed in a ^{3}He-^{4}He dilution fridge with a base electron temperature of 75 mK. Inside the dashed square in Fig. 1(a) we show a schematic circuit diagram of the on-chip components of the full Josephson junction. The fabrication is similar to Ref. 18. The superconductor-nanotube-superconductor junction is represented by a Josephson element (cross), a junction resistor R_J, and a junction capacitor C_J. The Josephson element has a current-phase relation, which we in the fitting procedure (see below) assume to be $I(\phi)=I_C \sin(\phi)$, with ϕ as the phase difference between the two superconducting and I_C as the critical current. However, the sinusoidal form of this relation is not in general true and this may cause some inaccuracy in the determination of the critical current. In Ref. 18, we show that the difference between the extracted I_C using either $\sin(\phi)$ or the correct functional form of the current-phase relation is in fact small and moreover largest near the 0-π transition relevant only for closed dots. We therefore expect the simpler relation also to be a reasonable approximation in the case of open dots [which allows us to use the Ivanchenko-Zil'berman relation in Eq. (9)]. At subgap bias voltages, R_J accounts for current due to multiple Andreev reflections and at higher bias voltages it accounts for quasiparticle transport. The capacitance between the superconducting electrodes ($C_J \sim 5$ fF) and between bonding pads ($C \sim 1$ pF) is estimated as a parallel-plate capacitance through the back gate. We have fabricated long thin metal leads with a measured resistance of $R \sim 1$ kΩ between the bonding pads and the superconducting electrodes which, as will be shown later, is crucial for increasing the measurable critical current.

III. OPEN QUANTUM DOT

In Fig. 1(b) we show a bias spectroscopy plot of differential conductance versus source-drain voltage (V_{sd}) and gate voltage (V_{gate}). Regular conductance oscillations in both source-drain and gate voltages are seen due to tuning of successive energy levels in the dot, with a separation (level spacing) ΔE, on and off resonances. Bias spectroscopy plots with the leads in the normal state ($B=150$ mT) (not shown) show conductances at the resonances ranging from 2 to 3.5 e^2/h. That high conductance is only allowed when the degeneracy of each energy level is fourfold (spin and orbital) and when the broadening of each energy level $\Gamma=\Gamma_s+\Gamma_d$, where the $\Gamma_s/\hbar$ ($\Gamma_d/\hbar$) is the tunnel rate through the source (drain) barrier, is larger than the Coulomb repulsion energy for adding an electron to the dot (charging energy) $U_C=e^2/C$. This regime ($\Delta E > \Gamma > U_C$) is often called the Fabry-Pérot regime[3–6,17,21] and the dot is termed as an open quantum dot. We will now analyze the bias spectrum and extract energy parameters, tunnel couplings, and capacitances.

From the size of the Fabry-Pérot diamond we have the following three equations, where we apply the source-drain

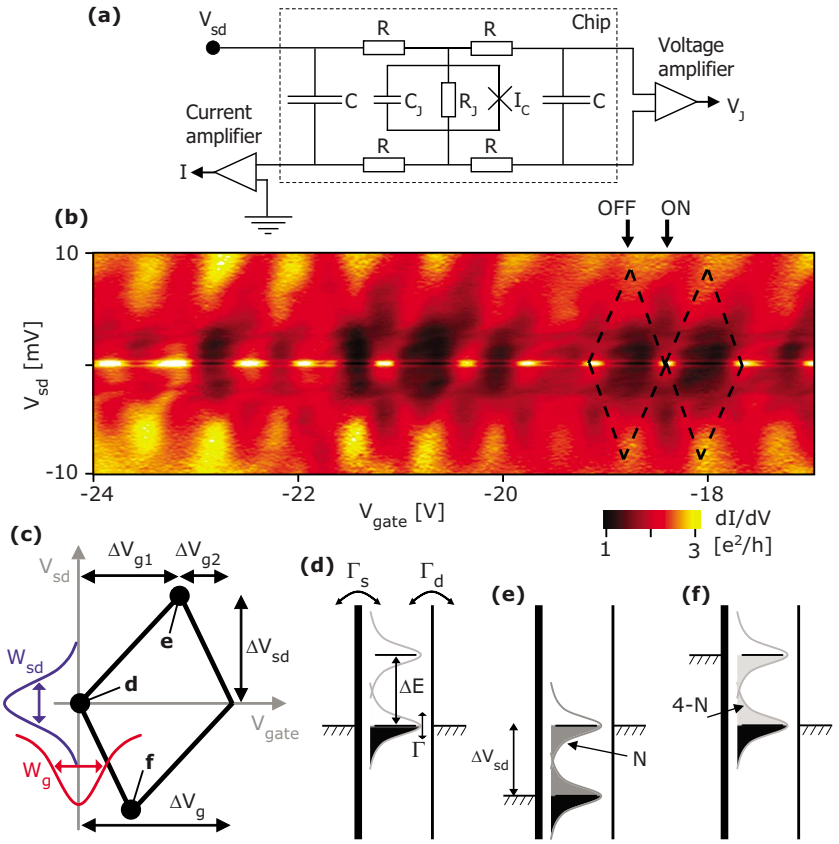

FIG. 1. (Color online) (a) Inside the dashed square: schematic circuit of on-chip components of the Josephson junction. Outside dashed square: four-probe voltage bias setup for ensuring junction voltage V_J vs current I. The full Josephson junction consists of both the superconductor-nanotube-superconductor junction, represented by a Josephson element I_C in parallel with a junction capacitor C_J, junction resistor R_J, on-chip resistors R, and capacitances C. (b) Bias spectroscopy plot of differential conductance versus source-drain and gate voltage. (c) Schematic of a Fabry-Pérot diamond. [(d)–(f)] Schematic transport diagrams at zero-bias resonance, positive-bias resonance, and negative-bias resonance.

voltage to the source electrode and keep the drain electrode at ground [see Figs. 1(c)–1(f)],

$$e\Delta V_{sd} = \Delta E, \tag{1}$$

$$e\frac{C_g}{C}\Delta V_g = \Delta E + 4U_C, \tag{2}$$

$$e\frac{C_g}{C}\Delta V_{g1} + e\frac{C_s}{C}\Delta V_{sd} = \Delta E + NU_C, \tag{3}$$

where e is the electron charge, ΔV_g, ΔV_{g1}, and ΔV_{sd} determine the size of the Fabry-Pérot diamond as shown in Fig. 1(c), and C_g, C_s, C_d, and C are the capacitance of the dot to gate, source, drain, and the total capacitance. N is the equilibrium number of electrons added to the dot from a zero-bias resonance to the first positive-bias resonance, i.e., from position d to e in Fig. 1. N can be given in terms of the tunnel barrier asymmetry ($\alpha = \Gamma_s/\Gamma_d$):

$$N = 4\frac{\Gamma_d}{\Gamma} = \frac{4}{\alpha + 1}, \tag{4}$$

where α can be found from the conductance at resonance: $G_0 = 16\alpha/(\alpha+1)^2 e^2/h$. For the resonance indicated with an arrow in Fig. 1(b) we find $G_0 \sim 2.6e^2/h$, $\alpha \sim 0.3$, and $N \sim 3.1$.

From the width (full width at half maximum) at resonances in gate (W_g) and bias (W_{sd}) [see Fig. 1(c)] we can set up the following two equations:

$$e\frac{C_g}{C}W_g = \Gamma + N'U_C, \tag{5}$$

$$eW_{sd} \approx 2\Gamma, \tag{6}$$

where the second equation is a good approximation when the asymmetry of the capacitive or tunnel coupling is not too large (see the Appendix). N' is the number of electrons added to the dot between $V_{\text{gate}} = \pm W_g/2$ from resonance. We estimate N' by integrating a Lorentzian density of state for each energy level on the dot:

$$N' = \int_{-W_g/2}^{W_g/2} \sum_j \frac{4}{\pi} \frac{\frac{1}{2}W_g}{(\epsilon + j\Delta V_g)^2 + \left(\frac{1}{2}W_g\right)^2} d\epsilon, \tag{7}$$

where the sum should include an appropriate number of energy levels. If only one energy level is included ($j=0$) $N'=2$ but for increasing number energy levels included N' saturates at a higher number (since the tails of the other levels contribute). For the device analyzed in paper it saturates at $N' \sim 2.5$.

By solving the equations above we can find expressions for the following parameters:

$$\Delta E = e\Delta V_{sd} \sim 9 \text{ meV},$$

$$U_C = \frac{W_g \Delta E - \frac{1}{2}e\Delta V_g W_{sd}}{N'\Delta V_g - 4W_g} \sim 0.5 \text{ meV},$$

$$C_g = \left(\frac{\Delta E}{U_C} + 4\right)\frac{e}{\Delta V_g} \sim 4.3 \text{ aF},$$

$$C_s = \frac{eC_g\Delta V_{g2} - (4-N)e^2}{\Delta E} \sim 152 \text{ aF},$$

$$C_d = \frac{e^2}{U_C} - C_s - C_g \sim 158 \text{ aF},$$

$$C = C_s + C_d + C_g \sim 315 \text{ aF},$$

$$\Gamma = \frac{W_{sd}}{2}e \sim 4.3 \text{ meV},$$

$$\Gamma_s = \Gamma\frac{\alpha}{\alpha+1} \sim 1 \text{ meV},$$

$$\Gamma_d = \Gamma\frac{1}{\alpha+1} \sim 3.3 \text{ meV}, \quad (8)$$

We have on the right-hand column estimated the parameters for the device analyzed in this paper.[22] Note that $\Delta E > \Gamma > U_C > \Delta_0$, where $\Delta_0 \sim 0.11$ meV is the superconducting energy gap (see below).

IV. JOSEPHSON JUNCTION

We now return to the measurements shown in Fig. 1(b), where two parallel conductance ridges are observed at low bias due to the density of states in the superconducting electrodes. The separation between these two rides is $4\Delta_0/e$, yielding $\Delta_0 \sim 0.11$ meV. In the following we focus on measurements performed on and off zero-bias resonance at the two indicated positions in Fig. 1(b). Current versus junction voltage (IV_J curves) off resonance for large scale voltages is shown in Fig. 2(a), where the black curve is with superconducting electrodes and the red curve is with a small magnetic field (150 mT) to suppress the superconductivity. At high bias $V_{sd} > 2\Delta_0/e$ transport is governed by quasiparticle transport and one Andreev reflection processes yielding an excess current, while at subgap bias $V_{sd} < 2\Delta_0/e$ transport are governed by Andreev reflections and supercurrent.[6] A closeup at very low bias voltages, shown in Fig. 2(b), reveals a pronounced supercurrent branch with finite resistance, a so-called diffusive supercurrent branch.[18] The black circles are measured with a voltage bias setup as shown in Fig. 1(a), while the green triangles are measured with a current bias setup (sweeping from negative to positive current). For voltage bias measurements we have observed no hysteresis or switching in the IV_J curves at any gate voltages. But for current bias measurements switching and hysteresis are observed whenever the full IV_J curve has local minima and maxima, as observed in Fig. 2(b). Such local minima and maxima will for current bias measurements lead to switching in voltage and result in a hysteretic IV_J curve. To resolve the full IV_J curve we have therefore used voltage bias measurements in this paper.

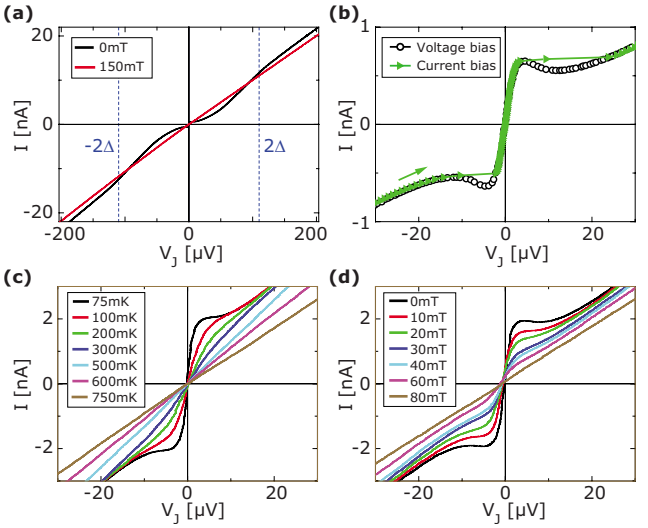

FIG. 2. (Color online) Current versus junction voltage [(a) and (b)] on and [(c) and (d)] off resonances at positions indicated in Fig. 1(b). (a) Black curve is with the electrodes in the superconducting state and red curve is with a small magnetic field (150 mT) applied to suppress the superconductivity. (b) Close up of the supercurrent branch from (a), measured with a voltage bias setup (circles) and a current bias setup (triangles). [(c) and (d)] Dependence of the diffusive supercurrent branch on (c) temperature and (d) magnetic field.

In Figs. 2(c) and 2(d) we show the temperature and magnetic-field dependence of the diffusive supercurrent branch, which we will analyze in the following. The zero-bias slope of the diffusive supercurrent branch in Fig. 2 yields a resistance on the order of kilohms. For a Josephson quantum dot junction with only two channels as for a nanotube the Josephson energy $E_J = \hbar I_C/2e$ can be comparable to the temperature of the cryostat. Thermal fluctuations will therefore lead to fluctuations in the phase difference across the junction and consequently give a supercurrent branch with finite resistance. In order to dampen these phase fluctuations and thereby increase the size of the supercurrent branch, we have designed the environment of the superconductor-nanotube-superconductor junction as described in Ref. 18. The quality factor for the junction is $Q < 0.5$, i.e., strongly damped. The full IV_J curve for a damped Josephson junction including the external components (without R_J) was calculated by Ivanchenko and Zil'berman[23] and used with great success by Steinbach *et al.*[20] Since this device has considerable current contribution from multiple Andreev reflections at subgap bias voltage we have a rough approximation included a constant resistor R_J. The full IV_J curve can then be calculated as[18]

$$I(V_{sd}) = I_C \,\mathrm{Im}\left(\frac{I_{1-\eta i}(E_J/k_BT)}{I_{-\eta i}(E_J/k_BT)}\right) + \frac{V_J}{R_J}, \quad (9)$$

where $I_n(x)$ is the modified Bessel function of complex order and $\eta = (\hbar V_{sd})/(2eRk_BT)$. To plot $I(V_{sd})$ versus V_J instead of V_{sd} we can use that $V_J = V_{sd} - RI(V_{sd})$. There are two fitting parameters in this theory, the temperature dependent critical current $I_C(T)$ and R_J. In Fig. 3 we show three I versus V_J

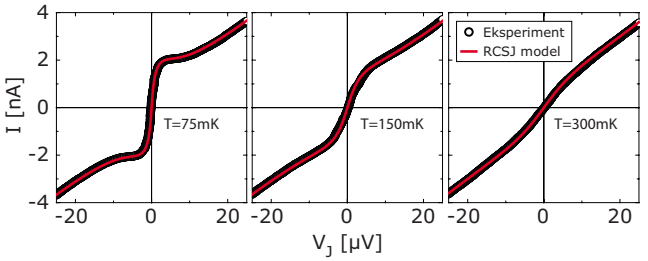

FIG. 3. (Color online) Current versus junction voltage on resonance at position indicated in Fig. 1(b) for three different temperatures. From left to right: 75, 150, and 300 mK. Four-probe voltage bias measurement (circles) and fit (solid red line) using Eq. (9) with R_J=7.7 kΩ and R=1 kΩ, the temperature at which the curve is measured, and I_C=4.8, 4.8, and 4.6 nA from left to right.

curves measured at the same gate voltage for increasing temperatures (from left to right: 75, 150, and 300 mK). The black circles are the measurement and the solid red curve is the theoretical fit with Eq. (9). The three fits are made with R_J=7.7 kΩ, and the temperature at which it is measured, the only free fitting parameter is $I_C(T)$ yielding 4.8, 4.8, and 4.6 nA, respectively. Equation (9) fits the measured IV_J curves very well for all temperatures with I_C as the only fitting parameter. Above ~300 mK smaller and smaller critical currents are needed to make a good fit. Critical currents versus temperature found by these fits are plotted in Fig. 4(a). At temperatures lower than ~300 mK the critical current is saturated at ~5 nA, while at higher temperatures it decreases more rapidly than a BCS-gap dependence. In Fig. 4(a) we also plot the excess current versus temperature, measured at $V_{sd}=4\Delta_0/e$. We compare the measurement with theory for a superconducting quantum point contact.[6,17,24–26] We use Eqs. 1 and 2 in Ref. 6 with $\Delta=\Delta(T)$ having a BCS-temperature dependence to fit the measured temperature dependence of the critical and excess current, solid red and blue curves in Fig. 4(a). The magnitudes of the measured critical and excess currents are 0.25 and 0.7 lower than the theory predicts, while their qualitative dependence on temperature fits well with theory.

In Fig. 4(b) we plot the magnetic-field dependence of the critical current on and off resonance [see arrows in Fig. 1(b)] and excess current on resonance. The critical currents are found by the same method as above by fitting Eq. (9) to each measured IV_J curve in Fig. 2(d). We compare the measurement to the same theory as above but with $\Delta=\Delta(B)=(1-B/B_C)\Delta_0$, where $B_C\sim 90$ mT is the critical field. We use a linear dependence because, as shown in the insert of Fig. 4(b), the subgap structure has approximately a linear dependence on magnetic field. The theory seems to fit qualitatively well to the measurement. But the magnitudes of the measured critical and excess currents are, as above for the temperature dependence, 0.25 and 0.7 lower than theory. Similar low values of critical[4,17,27] and excess currents[6] have recently been reported by several independent studies in the open quantum dot regime. In Ref. 4 the maximum critical current on resonance is slightly higher than reported above (7 versus 6 nA) consistent with a more symmetric coupling to the source and drain electrodes (higher on resonance conductance). The measurable critical current is almost identical to the critical current in their device, probably due to good filtering, in contrast to the lower value observed in our case. Most importantly, the overall magnitude of the critical current in both studies are suppressed compared to the values predicted by noninteracting theory.[28]

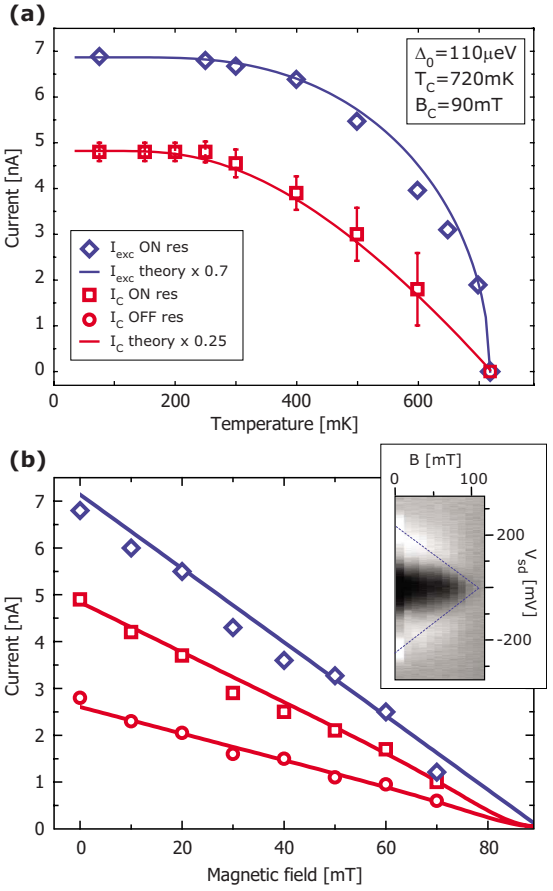

FIG. 4. (Color online) (a) Temperature dependence of the measured critical current (squares) and excess current (diamonds) on resonance. (b) Magnetic-field dependence of the measured critical current on and off resonance (squares and circles) and excess current on resonance (diamonds). The normal-state zero-bias conductance is $2.6e^2/h$ on resonance and $1.4e^2/h$ off resonance. The solid lines in both (a) and (b) are the predicted curves for a superconducting quantum point contact multiplied by a constant factor of 0.25 for the critical current and 0.7 for the excess current. Insert shows the magnetic-field dependence of the subgap structure of a similar device in the Coulomb-blockade regime.

V. CONCLUSION

In conclusion, we have studied the critical and excess current in a Josephson quantum dot junction realized in a carbon nanotube device. Using a fit to a model describing resonance tunneling through a set of resonances, we have extracted the device parameters. The parameters are consistent with the dot being in the open regime with tunneling coupling $\Gamma\sim 4$ meV and charging energy $U_C\sim 0.5$ meV so that $\Gamma\gg U_C$. The deduced charging energy is thus several

times larger than the superconducting energy gap (Δ_0=0.11 meV). We speculate that the observed discrepancy by a factor of 0.25 between the measured critical current and theoretically expected could be due to the charging energy being larger than the superconducting gap, giving rise to suppressed Cooper pair transport. Furthermore, the 0.7 discrepancy for the excess current has been observed before[6] and we have no good understanding of this but again the Coulomb interaction might play a role. Further theoretical understanding of this regime is therefore called for.

APPENDIX: MEAN-FIELD DESCRIPTION OF FABRY-PÉROT RESONANCES IN A NANOTUBE QUANTUM DOT

The electronic states in the nanotube can be described by

$$H_{cnt} = \sum_{m\eta\sigma} \Delta E n_{m\eta\sigma} + \frac{1}{2} U_C \tilde{N}^2 - eV_{\text{eff}}\tilde{N}, \tag{A1}$$

$$V_{\text{eff}} = \sum_{\beta=g,s,d} \frac{V_\beta C_\beta}{C}, \tag{A2}$$

where

$$\tilde{N} = \sum_{m\eta\sigma} n_{m\eta\sigma}, \quad U_C = \frac{e^2}{C}, \tag{A3}$$

and ΔE is the level spacing. The quantum numbers m, σ, and η describe the orbital, spin, and pseudospin degrees of freedom, respectively. The subscripts g, s, and d refer to gate, source, and drain. In the experiment we apply asymmetric bias, i.e., $V_s = V_{sd}$ and $V_d = 0$. In the mean-field approximation (which is valid when $\Gamma \gg U_C$), the Hamiltonian is

$$H_{cnt} \approx \sum_{m\eta\sigma} \Delta E n_{m\eta\sigma} + U_C \tilde{N}\langle\tilde{N}\rangle - eV_{\text{eff}}\tilde{N}, \tag{A4}$$

where the total occupation $\langle\tilde{N}\rangle$ should be determined self-consistently

$$\langle\tilde{N}\rangle = \sum_{m\eta\sigma} \langle n_{m\eta\sigma}\rangle, \tag{A5}$$

with

$$\langle n_{m\eta\sigma}\rangle = \sum_{\alpha=s,d} \frac{\Gamma_\alpha}{\Gamma} \int \frac{d\omega}{2\pi} n_F(\omega + eV_\alpha) A_{m\eta\sigma}(\omega). \tag{A6}$$

Assuming all levels to be simple Lorentzians with equal widths, the spectral functions are

$$A_{m\eta\sigma}(\omega) = \frac{\Gamma}{(\omega - m\Delta E - U_C\langle\tilde{N}\rangle + eV_{\text{eff}})^2 + (\Gamma/2)^2}. \tag{A7}$$

Inserting this into the integral, summing over quantum numbers, and setting $T=0$ then gives the self-consistency equation

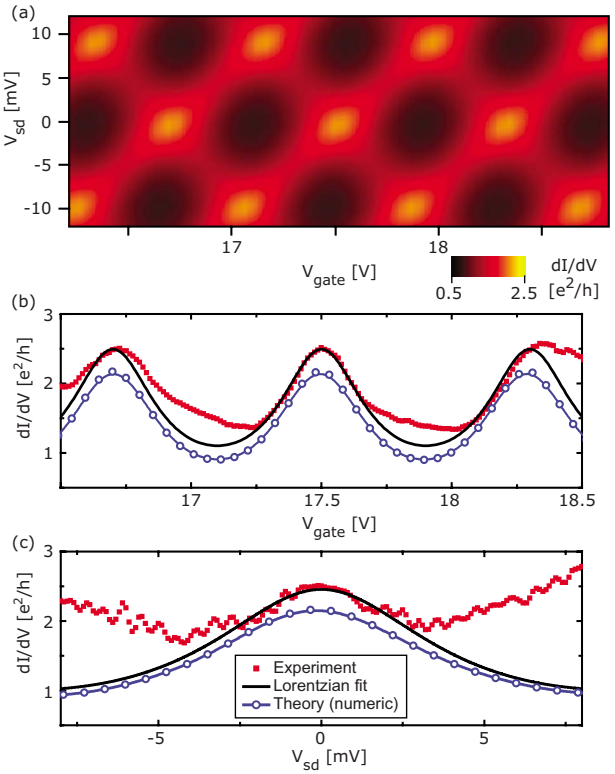

FIG. 5. (Color online) (a) Differential conductance versus bias and gate voltages using Eqs. (A8) and (A9). [(b) and (c)] Differential conductance versus gate voltage at V_{sd}=0 mV and versus bias voltage at resonance (c). Red squares are experimental data (measured with B=150 mT), solid black line is a Lorentzian fit to the measurement yielding W_g=0.4 V and W_{sd}=8.5 mV, and blue circles are numerical theory extracted from (a).

$$\langle\tilde{N}\rangle = \sum_m \sum_{\alpha=s,d} \frac{4\Gamma_\alpha}{\Gamma}\left[\frac{1}{2} - \frac{1}{\pi}\tan^{-1} \times\left(\frac{m\Delta E + eV_\alpha + U_C\langle\tilde{N}\rangle - eV_{\text{eff}}}{\Gamma/2}\right)\right]. \tag{A8}$$

This equation can be solved numerically. Once we know the total occupation for the given gate, source, and drain voltages, the current is given by

$$I = \frac{e}{h}\frac{4\Gamma_s\Gamma_d}{\Gamma}\sum_{m\eta\sigma}\int\frac{d\omega}{2\pi}[n_F(\omega + eV_s) - n_F(\omega + eV_d)]A_{m\eta\sigma}(\omega)$$
$$= \frac{4e}{h}\frac{4\Gamma_s\Gamma_d}{\pi\Gamma}\sum_m\left[\tan^{-1}\left(\frac{m\Delta E + eV_d + U_C\langle\tilde{N}\rangle - eV_{\text{eff}}}{\Gamma/2}\right) - \tan^{-1}\left(\frac{m\Delta E + eV_s + U_C\langle\tilde{N}\rangle - eV_{\text{eff}}}{\Gamma/2}\right)\right]. \tag{A9}$$

In Fig. 5(a) we plot the differential conductance versus bias and gate voltage using Eqs. (A8) and (A9) with the parameters found in Eq. (8). We compare the theory with experimental data measured with=150 mT in Figs. 5(b) and 5(c). In (b) we make a gate trace at zero bias and in (c) we make a bias trace at the resonance indicated in Fig. 1(a).

*hij@fys.ku.dk
†Present address: NTT Basic Research Laboratories, 3-1 Morinosato Wakamiya, Atsugi-shi, 243-0198 Kanagawa, Japan.

[1] A. Y. Kasumov, R. Deblock, M. Kociak, B. Reulet, H. Bouchiat, I. I. Khodos, Y. B. Gorbatov, V. T. Volkov, C. Journet, and M. Burghard, Science **284**, 1508 (1999).
[2] I. Takesue, J. Haruyama, N. Kobayashi, S. Chiashi, S. Maruyama, T. Sugai, and H. Shinohara, Phys. Rev. Lett. **96**, 057001 (2006).
[3] J.-P. Cleuziou, W. Wernsdorfer, V. Bouchiat, T. Ondarçuhu, and M. Monthioux, Nat. Nanotechnol. **1**, 53 (2006).
[4] J.-P. Cleuziou, W. Wernsdorfer, S. Andergassen, S. Florens, V. Bouchiat, T. Ondarçuhu, and M. Monthioux, Phys. Rev. Lett. **99**, 117001 (2007).
[5] P. Jarillo-Herrero, J. A. van Dam, and L. P. Kouwenhoven, Nature (London) **439**, 953 (2006).
[6] H. I. Jorgensen, K. Grove-Rasmussen, T. Novotny, K. Flensbert, and P. E. Lindelof, Phys. Rev. Lett. **96**, 207003 (2006).
[7] E. Pallecchi, M. Gaaß, D. A. Ryndyk, and C. Strunk, Appl. Phys. Lett. **93**, 072501 (2008).
[8] Y. Zhang, G. Liu, and C. N. Lau, Nano Res. **1**, 145 (2008).
[9] A. Morpurgo, J. Kong, C. M. Marcus, and H. Dai, Science **286**, 263 (1999).
[10] Y.-J. Doh, J. A. van Dam, A. L. Roest, E. P. A. M. Bakker, L. P. Kouwenhoven, and S. D. Franceschi, Science **309**, 272 (2005).
[11] C. Buizert, A. Oiwa, K. Shibata, K. Hirakawa, and S. Tarucha, Phys. Rev. Lett. **99**, 136806 (2007).
[12] A. Eichler, M. Weiss, S. Oberholzer, C. Schönenberger, A. Levy Yeyati, J. C. Cuevas, and A. Martín-Rodero, Phys. Rev. Lett. **99**, 126602 (2007).
[13] M. R. Buitelaar, W. Belzig, T. Nussbaumer, B. Babić, C. Bruder, and C. Schönenberger, Phys. Rev. Lett. **91**, 057005 (2003).
[14] M. R. Buitelaar, T. Nussbaumer, and C. Schönenberger, Phys. Rev. Lett. **89**, 256801 (2002).
[15] K. Grove-Rasmussen, H. Ingerslev Jørgensen, and P. E. Lindelof, New. J. Phys. **9**, 124 (2007).
[16] T. Sand-Jespersen, J. Paaske, B. M. Andersen, K. Grove-Rasmussen, H. I. Jorgensen, M. Aagesen, C. B. Sorensen, P. E. Lindelof, K. Flensberg, and J. Nygard., Phys. Rev. Lett. **99**, 126603 (2007).
[17] F. Wu, R. Danneau, P. Queipo, E. Kauppinen, T. Tsuneta, and P. J. Hakonen, Phys. Rev. B **79**, 073404 (2009).
[18] H. I. Jørgensen, T. Novotný, K. Grove-Rasmussen, K. Flensberg, and P. E. Lindelof, Nano Lett. **7**, 2441 (2007).
[19] J. A. van Dam, Y. V. Nazarov, E. P. A. M. Bakker, S. D. Franceschi, and L. P. Kouwenhoven, Nature (London) **442**, 667 (2006).
[20] A. Steinbach, P. Joyez, A. Cottet, D. Esteve, M. H. Devoret, M. E. Huber, and J. M. Martinis, Phys. Rev. Lett. **87**, 137003 (2001).
[21] W. Liang, M. Bockarth, D. Bozovic, J. H. Hafner, M. Tinkham, and H. Park, Nature (London) **411**, 665 (2001).
[22] ΔV_g=0.8 V ΔV_{g1}=0.45 V, ΔV_{g2}=0.35 V, ΔV_{sd}=9 mV, W_g=0.4 V, and W_{sd}=8.5 mV.
[23] Y. M. Ivanchenko and L. A. Zil'berman, Sov. Phys. JETP **28**, 1272 (1969).
[24] A. Martin-Rodero, A. Levy Yeyati, and J. C. Cuevas, Superlattices Microstruct. **25**, 925 (1999).
[25] V. S. Shumeiko, E. N. Bratus, and G. Wendin, Low Temp. Phys. **23**, 181 (1997).
[26] J. C. Cuevas, A. Martín-Rodero, and A. L. Yeyati, Phys. Rev. B **54**, 7366 (1996).
[27] G. Liu, Y. Zhang, and C. N. Lau, Phys. Rev. Lett. **102**, 016803 (2009).
[28] C. W. J. Beenakker, *Transport Phenomena in Mesoscopic Systems* (Springer, Berlin, 1992); arXiv:cond-mat/0406127 (unpublished)